Application of Imaging-Grazing-Incidence X-ray Diffraction and Specular Reflectivity to the Structural Investigation of Quantum-Confinement Semiconductor Devices

S. A. Holt,[a] A. S. Brown,[b] D. C. Creagh[c]* and R. Leon[d]

[a]School of Physics, University College, The University of New South Wales, Northcott Drive, Canberra, ACT 2600, Australia, [b]Research School of Chemistry, Australian National University, Canberra, ACT 0200, Australia, [c]Faculty of Information Science and Engineering, University of Canberra, PO Box 1, Belconnen, ACT 2616, Australia, and [d]Research School of Physical Sciences and Engineering, Australian National University, Canberra, ACT 0200, Australia. E-mail: dudleyc@ise.canberra.edu.au

X-ray reflectivity and grazing-incidence X-ray diffraction techniques have been employed to investigate the structure of quantum-well and quantum-dot semiconductor devices. This work has been performed using both laboratory and synchrotron radiation sources. The use of synchrotron radiation enabled reflectivity studies to be performed on small samples, and established the feasibility of imaging-grazing-incidence diffraction studies on quantum-confinement structures. Interdiffusion effects in quantum-well and quantum-dot structures, the disordering of overlayers grown on quantum dots, and the variation in diffraction pattern with incident angle have been observed. It is evident that X-ray reflectivity and imaging-grazing-incidence X-ray diffraction yield quite different but complementary information.

1. Introduction

X-ray reflectivity (XRR) and grazing-incidence X-ray diffraction (GIXD) provide powerful means for investigating the structures of surfaces, thin films and interfaces over length scales ranging from about 3 to 3000 Å. These techniques are finding widespread and increasing use in a variety of research areas such as, the study of Langmuir films at the liquid/air interface, solid polymer films, membranes, liquid surfaces, quantum-well (QW), multiple-quantum-well (MQW) and quantum-dot (QD) devices, thin metal films and semiconductor materials. XRR and GIXD are based on geometries in which X-rays impinge on the sample at very small angles of incidence. The refractive index of the sample is usually such that there is a critical angle of incidence below which the total reflection of X-rays occurs. Increasing the angle of incidence above the critical angle results in reflection and refraction of the X-rays, the details of which are related to the variation of refractive index in the sample. As the refractive index is related to the scattering-length density of the material (the product of the electron density and the classical electron radius), the reflectivity is a function of the composition variation through the sample.

XRR and GIXD have a number of advantages which make their use very attractive to the semiconductor industry. The application of XRR and GIXD in the investigation of QW, QD and MQW devices, for example, is complemen-tary to their study by transmission electron microscopy and atomic force microscopy. However, neither transmission electron microscopy nor atomic force microscopy are capable of providing direct information on a working device, and both techniques are inherently restricted to small fields of view. Structural information (including interface structure) can be obtained by transmission electron microscopy either by producing thin slices perpendicular to the growth direction or by preparing plan-view transmission electron microscopy specimens to visualize QD structures in the sample plane. Both these methods require time-consuming and destructive sample preparation methods, and thinning of samples may lead to modifications of the strain fields at the device interfaces (Shechtman, van Heerden & Josell, 1994). Atomic force microscopy can be used to study the distribution of quantum dots on a surface, but the surface will require cleaning before the device is capped, and the influence of etching, capping and annealing will necessarily alter the morphology of the quantum dots. In contrast, sample preparation for XRR and GIXD is straightforward and does not require the sacrifice of valuable material, or introduce artefacts through invasive preparative techniques. Because the methods rely on the interaction of X-radiation with matter, the samples are never physically disrupted as they may be with other techniques.

Quantum-confinement devices are currently the focus of considerable attention by the semiconductor industry, with significant advances being made in the design and

fabrication of such devices. The precise control of growth conditions, available with techniques such as metal–organic chemical vapour deposition (MOCVD) and molecular-beam epitaxy, have permitted rapid progress and the implementation of practical applications with quantum-confinement devices. Recent work has shown that intermixing or interdiffusion of the interfaces plays a significant role in determining the optical properties of QD (Leon et al., 1996) and QW (Leon et al., 1997) structures. A more detailed structural investigation of intermixed devices is necessary to clarify the interdiffusion mechanism and to provide information on changes in the morphology and interface of these structures. XRR and GIXD have the potential to provide useful information on the interfacial structures of these devices in a nondestructive manner.

This paper presents the results of reflectivity experiments performed on QD, QW and MQW structures with a rotating-anode source and synchrotron radiation. We also present the results of imaging-grazing-incidence X-ray diffraction (IGIXD) experiments on QD, QW and MQW structures obtained with synchrotron radiation, highlighting the advantages of IGIXD and the wealth of information that can be obtained with a relatively short exposure time. We demonstrate that by performing only specular reflectivity it is possible to miss important features of the system. This is clearly evident from off-specular results obtained using image-plate detection methods, in which the diffraction images can be obtained below and near the critical angle with exposure times of less than 2 min.

2. Experimental

The cross-sectional structure of the QD and QW structures is illustrated in Fig. 1. Hetero-epitaxic growth of these structures was achieved by MOCVD at 76 Torr in a laminar flow cell designed to enable large areas of uniform growth. The deposition materials were provided by precisely controlled flow rates of the following source gases: $(CH_3)_3Ga$, $(CH_3)_3In$, $(CH_3)_3Al$ and AsH_3. The hydrogen carrier flow rate was 17.5 standard $l\,min^{-1}$. The flow of $(CH_3)_3In$ was monitored and controlled by an EPISON ultrasonic sensor.

Two slightly different MQW samples, NC419 and NC420, were grown on Si (111) substrates cut 2° off-axis. In both samples the underlying MQW region consisted of $Al_{0.38}Ga_{0.62}As$ wells with AlAs barriers, finished with a single $Al_{0.55}Ga_{0.45}As$ layer (see Fig. 1a). The growth temperature was 1023 K. The difference between the samples was in the capping layer; in one (NC419) this was Zn-doped p-type GaAs (848 K) while in the other (NC420) it was Si-doped n-type GaAs (1023 K).

The QD structures were grown as follows: after growth of a GaAs buffer layer at 923 K on semi-insulating on-axis (100) GaAs substrates, the temperature was lowered to 823 K and quantum dots, in the form of nanometre-size InGaAs islands, were grown by depositing 4.5 monolayers (nominally) of $In_{0.49}Ga_{0.51}As$. A GaAs capping layer was then grown at 823 K. For the InGaAs QW sample, only

4 monolayers were deposited avoiding the strain-induced structural transformation to islands, retaining the layer structure. The pre-annealing average diameters and areal concentrations of quantum dots were 33 nm and $9 \times 10^9\,cm^{-2}$, respectively. Two QD and QW samples were selected for analysis, with one of each then being annealed in an argon atmosphere in a rapid thermal annealer at 1223 K for 30 s.

The Research School of Chemistry (RSC) reflectometer has been described elsewhere (Jamie, Dowling, Holt & Creagh, 1995). The incident angle is defined by the position of the sample stage which remains horizontal at all times. The Cu $K\alpha$ X-rays were produced by an Elliott GX-13 rotating-anode generator, the outlet port dimensions of which limit the incident angle to a maximum of $3.4°$ $(0.48\,\text{Å}^{-1})$. Specular scans were performed by setting the incident and exit angles equal and counting for a prescribed period of time; this process was repeated over the angular range measured with a predetermined step size between each data point.

The synchrotron radiation experiments were performed at the Australian National Beamline (BL20B) at the Photon Factory, KEK, Tsukuba, Japan. The specimen was mounted on the Q axis of BIGDIFF, a unique vacuum diffractometer (Barnea, Creagh & Davis, 1992), enabling control of the orientation of the specimen on two orthogonal arcs, as well as control of the height of the specimen in the beam (the z direction). The primary elements of

```
                 Air
        ┌──────────────────────┐
        │   Capping layer      │  ↕ 100 Å
        ├──────────────────────┤
        │   AlGaAs             │  ↕ 100 Å
        ├──────────────────────┤
   40   │   AlAs              │  ↕ 50 Å
repeats ├──────────────────────┤
        │   AlGaAs            │  ↕ 73 Å
        ├──────────────────────┤
        │   AlAs              │  ↕ 50 Å
        └──────────────────────┘
              Si substrate
                  (a)

                 Air
        ┌──────────────────────┐
        │   GaAs overlayer     │  ↕ 580 Å
        ├──────────────────────┤
        │   InGaAs            │  ↕ 10 Å
        └──────────────────────┘
              GaAs substrate
                  (b)

                 Air
        ┌──────────────────────┐
        │   GaAs overlayer     │  ↕ 580 Å
        ├──────────────────────┤
        │ InGaAs    InGaAs    │  ↕ 90 Å
        ├──────────────────────┤
        │   InGaAs            │  ↕ 10 Å
        └──────────────────────┘
              GaAs substrate
                  (c)
```
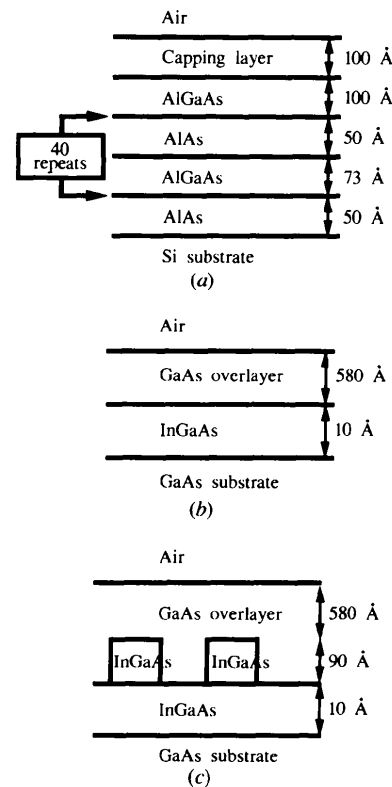
Figure 1
Schematic diagrams of the (a) MQW, (b) QD and (c) QW structures.

BIGDIFF as applicable to the XRR and IGIXD experiments under discussion can be seen schematically in Fig. 2. The wavelength of the incident radiation was set by the sagittal focusing monochromator, which consists of a fixed-exit height-separated-element double-crystal spectrometer incorporating silicon (111) crystals in which the second crystal can be bent by a four-point bender, focusing the horizontal beam by a factor of more than 20 (Creagh & Garrett, 1995). The wavelength was set at 1.7390 Å for the IGIXD and 1.1709 Å for the reflectivity experiments, with the monochromator system detuned to minimize third-order and higher harmonics.

Reflectivity measurements were made on the MQW samples with the RSC reflectometer. The QD and QW samples at this stage of the project are only available in small pieces (<8 × 8 mm) which could be measured at the RSC, but the convolution of beam footprint effects at low angles would make sensible analysis of the data almost impossible. The high brightness of synchrotron radiation enables the use of much smaller vertical slits (35 μm compared with 200 μm), constraining the beam footprint to

the sample area. For both instruments the data presented are composite profiles, consisting of sections collected using appropriate attenuation to limit the maximum count rate, each of which was then scaled accordingly to produce the final profile. The data were placed on an absolute reflectivity scale by dividing the count rate at each data point by the count rate at the critical angle (where the reflectivity should be unity).

For reflectometry experiments at BL20B, a scatter-slit was mounted between the specimen and a Radicon scintillation detector. The samples were held on an aluminium sample holder by teflon slides, and mounted inside BIGDIFF. These scans were performed in a number of sections, with a small step size selected around the critical angle (where the reflectivity is rapidly decreasing) and larger steps selected at higher Q values where the reflectivity decreases more slowly. The data collection was achieved by performing a rocking curve around each incident angle ($\pm 0.040°$ with 55 data points and a counting time typically of 0.5 or 1 s point^{-1}) with the maximum of the specular peak taken as the reflectivity.

(a)

(b)
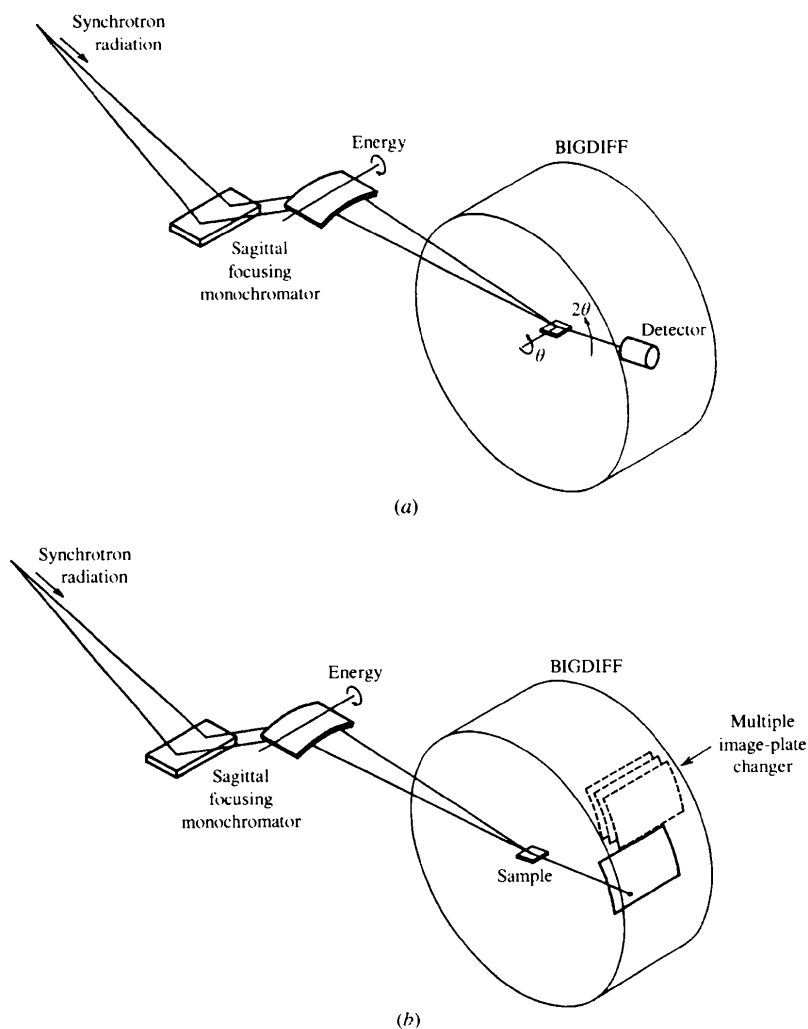
Figure 2
Schematic representation of the experimental configuration employed at BL20B: (a) XRR and (b) IGIXD.

For IGIXD experiments a beam-stop was positioned behind the specimen to prevent spillover of the direct beam onto the image plates. This restricted the smallest observable Q value to approximately 0.01 Å^{-1}. The image plates were located 400 mm from the specimen with the long dimension parallel to the xy plane of the sample. The positioning of the image plates was such that the direct beam would have intersected in the lower left corner. Up to ten imaging plates could be mounted in the recently constructed image-plate changer (Foran et al., 1997) designed for use in GIXD experiments involving thin multilayer films.

IGIXD was performed on MQW (NC420) and all QD and QW samples described previously. The incident angles were fixed and the image plates exposed for specified times. Five incident angles were used for each sample, 0.034, 0.1, 0.2, 0.3 and 0.4 Å^{-1}. The exposure times ranged from 2 min at lowest Q through to 10 min at highest Q. After exposure the image plates were scanned in a BAS 2000 image-plate reader (Fuji). The data presented in this paper have undergone minimal processing (background subtraction only).

3. Results and comments

Specular reflectivity profiles recorded at the RSC for the two MQW structures are shown in Fig. 3. The samples are ostensibly the same, differing only in the doping of the GaAs overlayer. The major features observed are the Bragg peaks which arise from the repeated AlAs/AlGaAs layers in the structure. Kiessig fringes corresponding to the total thickness are not observed, as they are beyond the resolution of the instrument. Also shown in Fig. 3 is a simulated reflectivity profile using the layer thicknesses given in Fig. 1, scattering-length densities calculated from the known compositions and estimated physical densities of the layers, Gaussian roughnesses of 3.0 Å at each interface, a Gaussian resolution function based on a $\Delta\theta$ of 0.01356°
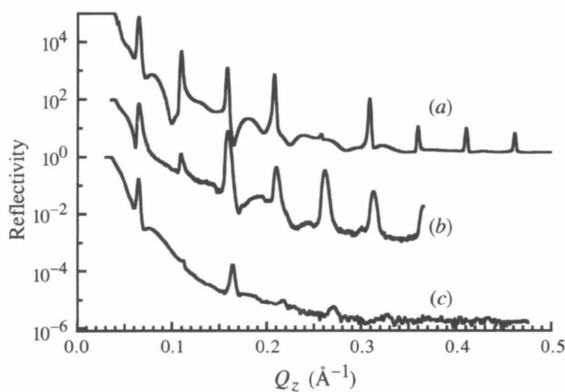
and a constant background of 1.5×10^{-5}. A number of the features are common to the experimental profile and the simulation, notably the Bragg peaks, shoulders between the peaks and the peak asymmetries. There are some notable discrepancies between experiment and simulation, particularly the much reduced intensity of the peak at approximately 0.26 Å^{-1} in the simulated profile. The spacing calculated for sample NC419 (Fig. 3b) was 122.2 Å, compared with the expected value of 123 Å. While the features from the reflectivity profile of sample NC420 (Fig. 3c) are similar to NC419, they are not as well defined with the apparent layer spacing being smaller (117.7 Å).

Examples of IGIXD from sample NC420 with the incident angle set below and above the critical angle can be seen in Fig. 4. Fig. 4(a) includes the entire image plate, illustrating the range of scattering vector readily accessible. Subsequent image plates have been truncated to display the full height and left-hand side of the image plate. The range of scattering vector on the full image plate extends to 3.01 Å^{-1} along the Q_z direction and 4.53 Å^{-1} to the right and 1.38 Å^{-1} to the left of the $Q_{xy} = 0$ position. We shall refer to the region of the image plate directly above the $Q_{xy} = 0$ position as the extended reflectivity region, as it is an extension of the region of Q space which is sampled in a specular reflectivity experiment. All subsequent IGIXD data presented have been restricted to the left-hand side of the image plate.

Below the critical angle (Fig. 4a) there exists a strong extended reflectivity region. In the lower section of this

Figure 3
Specular reflectivity profiles for the MQW structures illustrated in Fig. 1. (a) Simulation as described in the text. Experimental data recorded at the RSC for samples with (b) n-doped (NC419) and (c) p-doped (NC420) GaAs capping layers. The profiles have been arbitrarily offset for clarity.
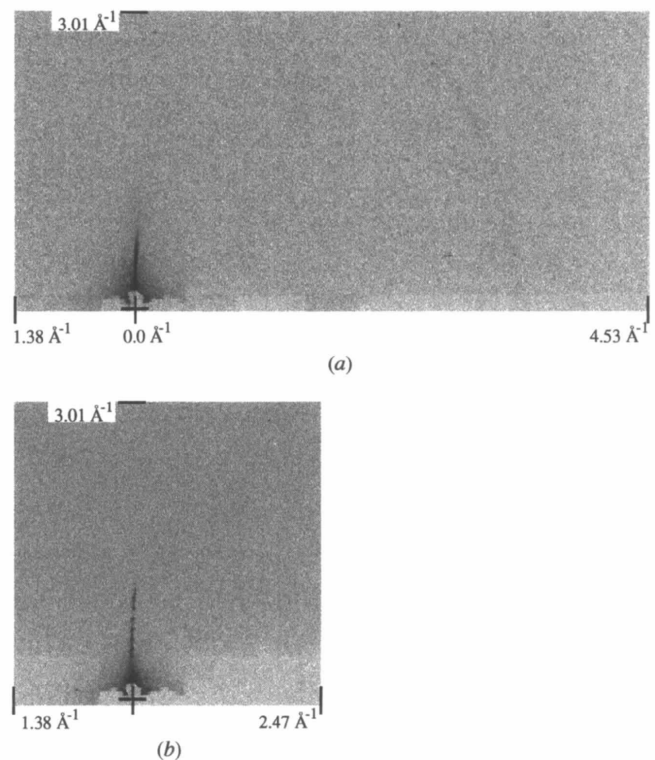
Figure 4
IGIXD patterns from the NC420 MQW structure. (a) An incident angle of 0.034 Å^{-1} and (b) an incident angle of 0.40 Å^{-1}.

region two strong reflections are observable if the image threshold is increased sufficiently. Fig. 4(b) shows a section of the image plate recorded above the critical angle, with the extended reflectivity region magnified. In these enlargements quasi-Bragg scattering is observed due to the alternation of layers in the MQW structure.

Notable in this image is the bending of the extended reflectivity away from the specular reflection direction and the streaking and misplacement of the quasi-Bragg spots with respect to the average intensity. The first we attribute to warping or delamination of the epilayer with respect to the substrate. The second may be explained by strains in layers being slightly different from layer to layer. XRR is sensitive to information only in the Q_z direction; consequently, deviations resultant from strain or delamination could account for the differences observed in the reflectivity profiles in Figs. 3(b) and 3(c).

Specular reflectivity profiles for QD and QW structures collected at BL20B are shown in Fig. 5. The Kiessig fringes evident in the unannealed QD structure (Fig. 5a) indicate that there is a pronounced scattering-length density difference between the layers of the sample. After annealing the amplitude of the Kiessig fringes has been suppressed, indicating either interface roughening or a marked decrease in the scattering-length density difference between the layers. These two processes (particularly the former) could be induced by interdiffusion of material between the layers during annealing. This result, which has been inferred from photoluminescence studies of similar samples (Leon *et al.*, 1996), is readily obtained from specular reflectivity studies. In addition, with more complete datasets and careful data analysis it should be possible to quantify the interface diffusion as a function of time for specific annealing temperatures, and to calculate the proportion of quantum dots in a layer. The specular reflectivity profile for the annealed QW structure displays more pronounced Kiessig fringes, but due to beam-time limitations a complete reflectivity

profile for the corresponding unannealed sample was not recorded.

A subset of the IGIXD data obtained on the unannealed QD and QW devices is presented in Figs. 6 and 7. Fig. 6 presents the IGIXD patterns obtained for the QD sample. The disordered nature of the surface layer can clearly be seen in Fig. 6(a), where a series of discrete dots, due to GaAs [111] crystal planes, is observed. It is important to note that the prevalence of these dots is greatly reduced with increased incident angle (Fig. 6b), and they were not evident on the unannealed QW (Fig. 7) nor were they observed on the annealed QD or QW samples (not shown). The disorder is evident in the unannealed QD structures, with the GaAs layer deposited onto a 'three-dimensional' surface, compared with deposition onto the QW layer. Also visible is scattering, evident at 45° either side of the specular direction, due to the [011] and the [0$\bar{1}$1] planes. A very similar feature, though not as pronounced, is also observed on the unannealed QW sample (Fig. 7a). The structure within the heavily exposed sections has yet to be fully analysed. Preliminary sections of the image show a disturbed diffuse-scattering intensity resulting from the interference diffuse scattering from the three truncation rods and the specular reflection. Above the

(a)   (b)
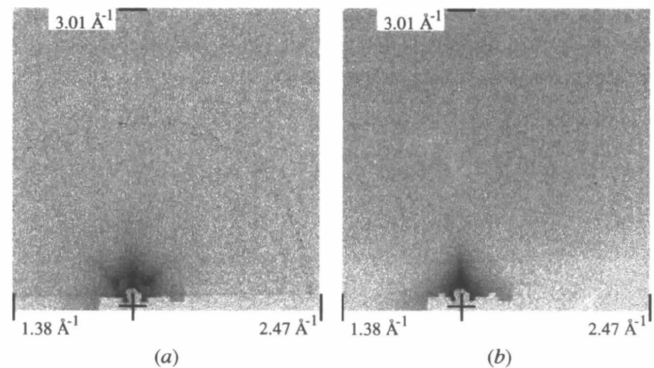
Figure 6
IGIXD patterns from the unannealed QD structure. (a) The full image plate at an incident angle of 0.034 Å^{-1} and (b) an incident angle of 0.40 Å^{-1}.

Figure 5
Specular reflectivity profiles for the QW and QD structures illustrated in Fig. 1. The profiles were recorded at BL20B. (a) Unannealed QD structure, (b) annealed QD structure and (c) annealed QW structure. The profiles have been arbitrarily offset for clarity.

(a)   (b)
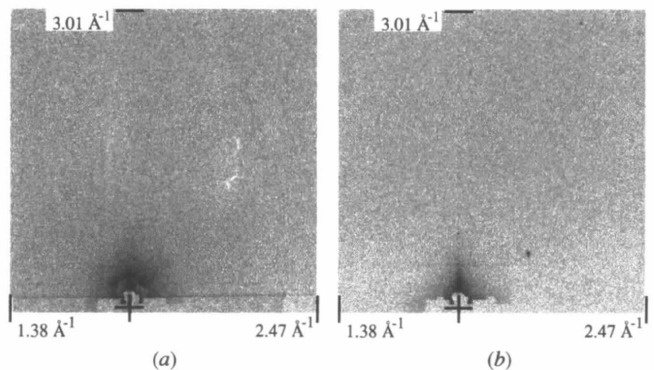
Figure 7
IGIXD patterns from the unannealed QW structure. (a) An incident angle of 0.034 Å^{-1} and (b) an incident angle of 0.40 Å^{-1}.

critical angle the effect of the surface disorder is much reduced. There are a number of strong reflections present (more prevalent at larger scattering vectors), believed to be due to Bragg reflections arising from dynamical scattering processes and/or contributions from the substrate scattering. These strong reflections were most noticeable on the IGIXD data recorded at high incident angle on the QW structures.

Detailed interpretation of the depth-resolved IGIXD series for each of the quantum-device samples (annealed and unannealed) will be the subject of subsequent publications.

4. Conclusions

In this paper we have demonstrated that IGIXD is an important complement to specular reflectivity measurements. The resolution of specular reflectivity, with our current configuration, exceeds that obtainable from IGIXD measurements. The IGIXD measurements, however, provide a wealth of information which is of great importance in many systems, that could not be obtained except by the performance of very time consuming triple-axis-type measurements.

Both the reflectivity and IGIXD measurements have demonstrated that it is relatively straightforward to distinguish between QD and QW devices of similar structure, and to observe the effects of annealing on the device structure. IGIXD profiling highlighted different structural aspects of the devices as the penetration depth of radiation into the structure was altered. The detailed results of this work will be presented in subsequent papers.

References

Barnea, Z., Creagh, D. C. & Davis, T. J. (1992). *Rev. Sci. Instrum.* **63**(1), 1068–1072.

Creagh, D. C. & Garrett, R. F. (1995). *Access to Major Facilities Program*, edited by J. W. Boldeman, pp. 251–252. ANSTO, Sydney, Australia.

Foran, G. J., Gentle, I. R., Peng, J. B., Barnes, G. T., Garrett, R. F. & Creagh, D. C. (1997). In preparation.

Jamie, I. M., Dowling, T. L., Holt, S. A. & Creagh, D. C. (1995). *3rd Vacuum Society of Australia Congress Proceedings*, pp. 25–27. University of Newcastle, Australia.

Leon, R., Kim, Y., Jagadish, C., Gal, M., Zou, J. & Cockayne, D. J. H. (1996). *Appl. Phys. Lett.* **69**(13). In the press.

Leon, R., Krueger, J., Melloch, M., Bozek, R., Wysmolek, A., Kurpiewski, A. & Kaminska, M. (1997). In preparation.

Shechtman, D., van Heerden, D. & Josell, D. (1994). *Mater. Lett.* **20**(5–6), 329–334.